J. Fluid Mech. (1972), *vol.* 56, *part* 2, *pp.* 337–351
Printed in Great Britain

Some properties of sink-flow turbulent boundary layers

By W. P. JONES† AND B. E. LAUNDER
Department of Mechanical Engineering, Imperial College, London

(Received 12 January 1972)

An experimental study of asymptotic sink-flow turbulent boundary layers is reported. Three levels of acceleration corresponding to values of the acceleration parameter K of $1{\cdot}5 \times 10^{-6}$, $2{\cdot}5 \times 10^{-6}$ and $3{\cdot}0 \times 10^{-6}$ have been examined. In addition to mean velocity profiles, measurements have been obtained of the profiles of longitudinal turbulence intensity, and, for the lowest value of K, of the lateral and transverse components as well. Measurements at selected positions in the boundary layer of the power spectral density indicate that none of the boundary layers exhibit an inertial subrange; for the steepest acceleration, in particular, throughout the boundary layer the spectrum shapes are similar in form to those reported within the viscous sublayer of a high Reynolds number turbulent flow.

1. Introduction

Turbulent flow through a plane-walled convergent channel is among the most interesting of the fundamental turbulent shear flows. The interest stems from the fact that such flows approach (and may sensibly attain) a form which is independent of streamwise position in which any Reynolds number based upon local velocity and length scales is constant (the velocity increasing downstream at the same rate as the boundary-layer thickness diminishes); the interesting corollary of that result is that there is no net entrainment of fluid into the boundary layer.

Coles (1957) perhaps made the earliest suggestion for the distribution of velocity in sink-flow boundary layers. At that time the view was widely held that the velocity profile in any turbulent boundary layer could be adequately represented as the sum of a 'wall component' and a 'wake component' (Coles 1956), the relative importance of these two components differing from one flow to another. According to Coles the sink flow provided an extreme class of boundary layer in which the wake component was zero; over the whole boundary layer outside the viscous-affected near-wall region, the velocity profile was thus supposed to possess the well-known semi-logarithmic form often referred to as the 'law of the wall'. Some years later Herring & Norbury (1967) provided measurements of an accelerating boundary layer in which, as we have argued elsewhere (Launder & Jones 1969), the flow properties were close to those of an asymptotic sink flow.

† Present address: Lehrstuhl für Technische Thermodynamik, Technische Hochschule, Aachen, West Germany.

Their velocity profiles indeed followed very closely a semi-logarithmic variation, providing substantial support for Coles's conjecture. These data were, however, for a flow with a quite modest level of acceleration.

We may characterize the strength of the acceleration by the magnitude of the parameter K, defined as $\nu/U^2\,(dU/dx)$, where U is the local free-stream velocity and ν the kinematic viscosity of the fluid†; in the Herring & Norbury experiments K was approximately $0{\cdot}2 \times 10^{-6}$. In the mid 1960's a number of workers discovered that K provided a reasonable indicator of whether or not turbulent boundary layers in nozzles would decay towards a laminar flow. The level of acceleration above which laminarization occurred was, in round terms, ten times as large as in the Herring & Norbury experiments. Thus, it seemed that the further examination of sink-flow boundary layers, with accelerations an order of magnitude greater than those previously considered, would yield information of much relevance to the laminarization problem in particular and to low Reynolds number turbulence in general.

Sink flows at higher levels of acceleration have been examined by Launder & Stinchcombe (1967), Jones (1967), Badri Narayanan & Ramjee (1968), Julien, Kays & Moffat (1969) and Loyd, Moffat & Kays (1970). In few of the above experiments did it appear that the boundary layers had reached their asymptotic state and the Launder & Stinchcombe data, in particular, were impaired by three-dimensional effects. Nevertheless, there is agreement among the experiments that there is no discernible 'universal' logarithmic region in the velocity profile for a value of K greater than about $1{\cdot}0 \times 10^{-6}$. Above this acceleration level, the thickness of the viscous sublayer increases progressively with K until a value is reached at which a turbulent shear flow can no longer be sustained. Loyd *et al.* (1970) suggest that the maximum value of K for turbulent flow is not greater than $2{\cdot}5 \times 10^{-6}$, whereas the data of Launder & Stinchcombe (1967) suggest the limit to be at least $3{\cdot}0 \times 10^{-6}$.

It is the purpose of the present paper to report further measurements of sink-flow boundary layers. Especial attention has been given to ensuring that the self-preserving form of the boundary layer is reached, to the measurement of wall shear stress and to the determination of those Reynolds stresses which were accessible to measurement with a hot-wire anemometer.

2. Apparatus, instrumentation and data processing

The experiments were carried out in an open-circuit wind tunnel which is fully described by Jones (1971). The working section is a 16 in. wide, 9 in. high, 72 in. long rectangular duct constructed from $\frac{1}{2}$ in. thick perspex sheets, a section of the roof of which can be set at any inclination to the lower wall; for the principal experiments the roof was set at 10° to the horizontal. The roof and lower wall (the test plate) thus form a two-dimensional plane convergent channel. The test plate, which has static pressure holes spaced at 2 in. intervals along its centreline, can be moved relative to the inclined roof and thus conditions (e.g. the local Reynolds number) at the start of the acceleration can be varied.

† In a sink flow K is thus invariant with respect to streamwise position.

Mean velocity profiles were measured along the centre-line of the test plate with a flattened-tip Pitot tube with tip dimensions 0·011 × 0·120 in. with a wall thickness of 0·003 in. The only correction made to the velocity measurements was a displacement correction similar to that proposed by McMillan (1956), whereby 15 % of the probe tip height was added to the distance between the probe and the wall. The dynamic and static pressures were measured with a null-reading tilting U-tube micromanometer which contains silicon fluid of specific gravity 0·822 and which is accurate to within $\pm 10^{-4}$ in. of fluid. A complete description of this instrument is given by Bradshaw (1965).

Wall shear stresses were determined by use of Stanton tubes made from stainless-steel razor blades. The tubes were glued to the plate and calibrated in a zero pressure gradient† against a Preston tube (using Patel's (1965) calibration). Readings were then taken in the constant-K flow, after which the Stanton tubes were removed.

Wall shear stresses were also obtained from the measured mean velocity profiles. For similar boundary layers the boundary-layer equation may be transformed into an ordinary differential equation and integrated (see Jones 1971) to yield

$$-\frac{\overline{uv}}{U^2} = K\int_\eta^\infty (1-f^2)\,d\eta - \frac{df}{d\eta}, \tag{1}$$

where f is the ratio of local to free-stream velocity, η is the normal distance Reynolds number, Uy/ν, u and v are the fluctuating components of velocity in the x and y directions and overbars denote the usual time averaging. By letting the lower limit of integration in (1) go to zero it follows that

$$\tfrac{1}{2}C_f = KR_2(H+1), \tag{2}$$

where C_f, R_2 and H are the conventionally defined skin-friction coefficient, momentum-thickness Reynolds number and shape factor respectively. This relation was used to determine C_f from the measured values of K, R_2 and H.

The hot-wire measurements were performed using the following equipment: two DISA constant-temperature anemometers type 55A01, two DISA linearizer units type 55D10, one DISA r.m.s. voltmeter type 55D35, one DISA random signal indicator and correlator type 55A06, one Solartron d.c. digital voltmeter type LM 1420.2, one Brüel & Kjaer audio frequency spectrometer type 2112, and one Tele-equipment oscilloscope type D53.

The longitudinal turbulence intensities were measured with a DISA gold-plated boundary-layer probe type 55F04 while for the transverse and normal intensities and shear stress the miniature X-wire type 55A38 was used. Calibration of the hot wire was performed immediately before each profile measurement. The only correction made to the hot-wire measurements was the tangential cooling correction of Champagne, Sleicher & Wehrmann (1967) which was applied to the X-wire measurements. The $\overline{u^2}$ spectra were measured with the Brüel & Kjaer frequency analyser operating on a bandwidth of $\frac{1}{3}$ octave. The measured frequency distributions were then transformed into wavenumber spectra by use of the identities

$$l \equiv 2\pi n/U_c, \quad F(l) \equiv (U_c/2\pi)\,G(n),$$

† The uniform pressure flow was achieved by raising the roof of the working section.

x (in.)	$K \times 10^6$	H	R_2	$\frac{1}{2}C_f^{(1)}$	$\frac{1}{2}C_f^{(2)}$
8	1·50	1·46	711	0·0026	0·0023
12	1·55	1·48	672	0·0026	0·0025
16	1·50	1·42	689	0·0025	0·0026
20	1·49	1·43	687	0·0025	0·0024
24	1·51	1·43	658	0·0024	0·0025
28	1·47	1·47	640	0·0023	0·0028

		Layer A		Layer B			
x (in.)	$K \times 10^6$	H	R_2	H	R_2	$\frac{1}{2}C_f^{(1)}$	$\frac{1}{2}C_f^{(2)}$
12	2·57	1·50	391	1·53	338	0·0022	—
16	2·54	1·50	387	1·56	345	0·0022	0·0022
20	2·45	1·51	383	1·55	358	0·0022	0·0022
24	2·47	1·56	361	1·60	332	0·0021	0·0024
28	2·50	1·62	339	1·62	342	0·0022	0·0025

		Layer I		Layer II		Layer III			
x (in.)	$K \times 10^6$	H	R_2	H	R_2	H	R_2	$\frac{1}{2}C_f^{(1)}$	$\frac{1}{2}C_f^{(2)}$
12	3·04	1·46	474	1·49	387	1·54	339	0·0026	—
16	3·00	—	—	—	—	1·59	305	0·0024	0·0025
20	2·90	1·48	416	1·55	369	1·62	319	0·0024	0·0023
24	2·96	—	—	—	—	1·63	303	0·0024	0·0021
28	2·02	1·56	368	1·65	312	1·76	276	0·0023	0·0023

TABLE 1. Variation of boundary-layer integral parameters in the constant-K acceleration. $\frac{1}{2}C_f^{(1)}$ = value of friction coefficient given by equation (2); $\frac{1}{2}C_f^{(2)}$ = value of friction coefficient obtained from Stanton tube measurements.

where n is frequency, l is wavenumber, $F(l)$ is the wavenumber spectrum and where $G(n)$ is the measured frequency distribution.

The convection velocity U_c was assumed equal to the local mean velocity.

3. Mean flow field

The variation through the convergent channel of the momentum-thickness Reynolds number, shape factor, skin-friction coefficient and acceleration parameter is given in table 1. For all three cases, K reaches a constant value at approximately 8 in. downstream from the convergent channel entrance and is maintained constant to within about 5 % over a distance of approximately 20 in. In all cases R_2, H and C_f remain sensibly constant in the region of constant K. The values of C_f obtained by use of the two-dimensional integral equation and directly by use of the Stanton tube agree within approximately ± 5 %. This result suggests that a satisfactorily two-dimensional flow has been attained.

At $K = 1{\cdot}5 \times 10^{-6}$, R_2, H and C_f have constant values of about 680, 1·50 and 0·0025 respectively throughout the region of constant K. For $K = 2{\cdot}5 \times 10^{-6}$ two experiments were taken with differential initial values of R_2 at the convergent-channel entrance. For the lower value, R_2 remains practically constant and H shows a small perceptible rise to a constant value of 1·6. For the higher initial value, R_2 decreases and the shape factor rises slowly through the acceleration.

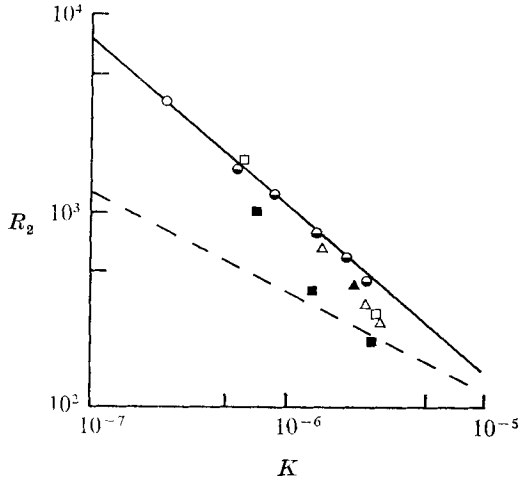

FIGURE 1. Variation of momentum-thickness Reynolds number with K for sink-flow boundary layers. ○, Herring & Norbury; □, Badri Narayanan & Ramjee; ■, Launder & Stinchcombe; ▲, Jones; ◒, Stanford data; △, present results; ——, turbulent solution; – – – –, laminar solution.

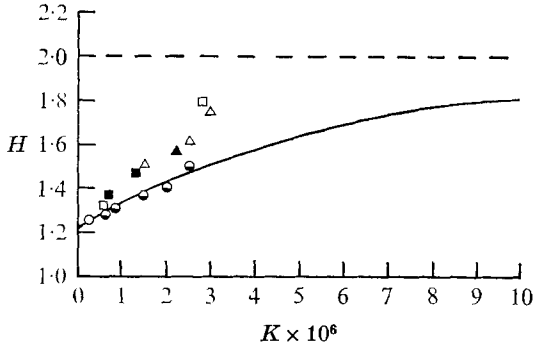

FIGURE 2. Variation of shape factor with K for sink-flow boundary layers. ○, Herring & Norbury; □, Badri Narayanan & Ramjee; ■, Launder & Stinchcombe; ▲, Jones; ◒, Stanford data; △, present results; ——, turbulent solution; – – – –, laminar solution.

At the end of the channel R_2 and H have the same values for each experiment; it thus seems reasonable to infer that the asymptotic state has been reached.

For the steepest acceleration, the variation of R_2 and H was documented for three different initial conditions. The experiments with the two highest initial values of R_2 show decreasing values of R_2 along the test plate. The flow arising from the thinnest initial boundary layer also displays a small progressive decrease in R_2 through the test section. Although here the changes in R_2 and H may fall within the error bounds of the measurements, we cannot with certainty conclude that the boundary layer has reached its asymptotic form by the end of the acceleration.

The variation of the asymptotic values of R_2 and H with K, shown in figures 1 and 2, provides a convenient basis for comparing the present data with those of other workers who have set up near-equilibrium sink flows. To facilitate

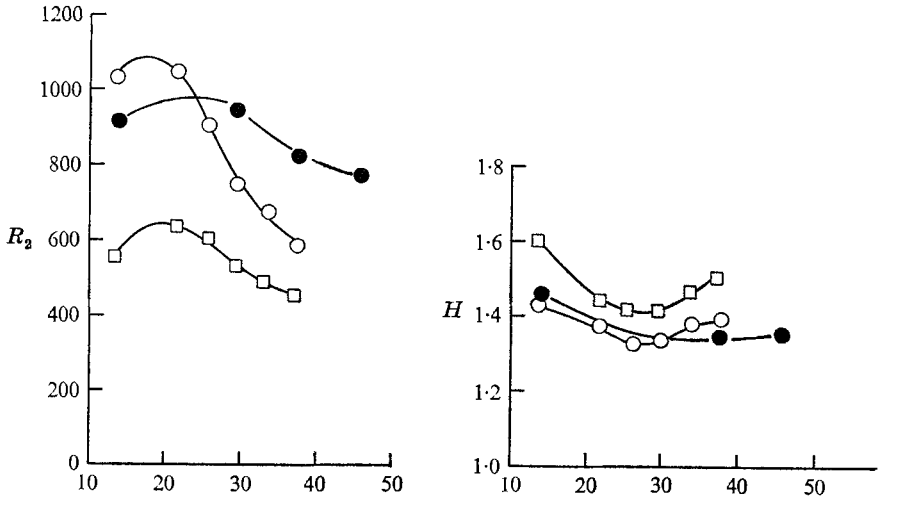

FIGURE 3. Stanford data: variation of integral parameters through the acceleration. ●, $K = 1{\cdot}44 \times 10^{-6}$; ○, $K = 2{\cdot}0 \times 10^{-6}$; □, $K = 2{\cdot}5 \times 10^{-6}$.

discussion of the various data the analytical solution appropriate to laminar flow is shown together with one obtained for turbulent flow which employed the Van Driest form of the mixing-length hypothesis (Launder & Jones 1969).

The results of Herring & Norbury, Julien *et al.*

$$(K = 0{\cdot}57 \times 10^{-6};\ K = 0{\cdot}77 \times 10^{-6})$$

and Badri Narayanan & Ramjee ($K = 0{\cdot}6 \times 10^{-6}$) are representative of similar boundary layers arising in a mild acceleration. For these layers the Reynolds number and shape factor H lie close to the mixing-length solution. This is not an unexpected result since the Reynolds numbers are relatively large; we should also not expect a mild pressure gradient to affect the turbulence structure of the boundary layer to any appreciable extent.

As figure 2 indicates, the data at higher acceleration levels divide into two groups: those of Julien *et al.* (1969) and Loyd *et al.* (1970) (obtained on the same apparatus) follow almost exactly the predicted mixing-length solution while the Badri Narayanan & Ramjee data and those of the present authors and their colleagues indicate a much faster approach towards the laminar value of H of about 2·0. A corresponding trend is shown in figure 1 (though here the Launder & Stinchcombe data are anomalously low because they are not two-dimensional).

We think that the cause of differences between the two groups of data is attributable to Julien's and Loyd's data not having attained the asymptotic form. Their tunnel, though excellent for many other purposes, was not well suited to the measurement of high-K sink flows because it possessed no independent means of adjusting the initial Reynolds number. Consequently, as figure 3 shows, the Reynolds number underwent appreciable variation through the test section.

The velocity profiles of the present study are now examined in greater detail. The normalized velocity f on linear scales is plotted versus the similarity variable η in figure 4. The velocity profiles for each value of K exhibit small changes in

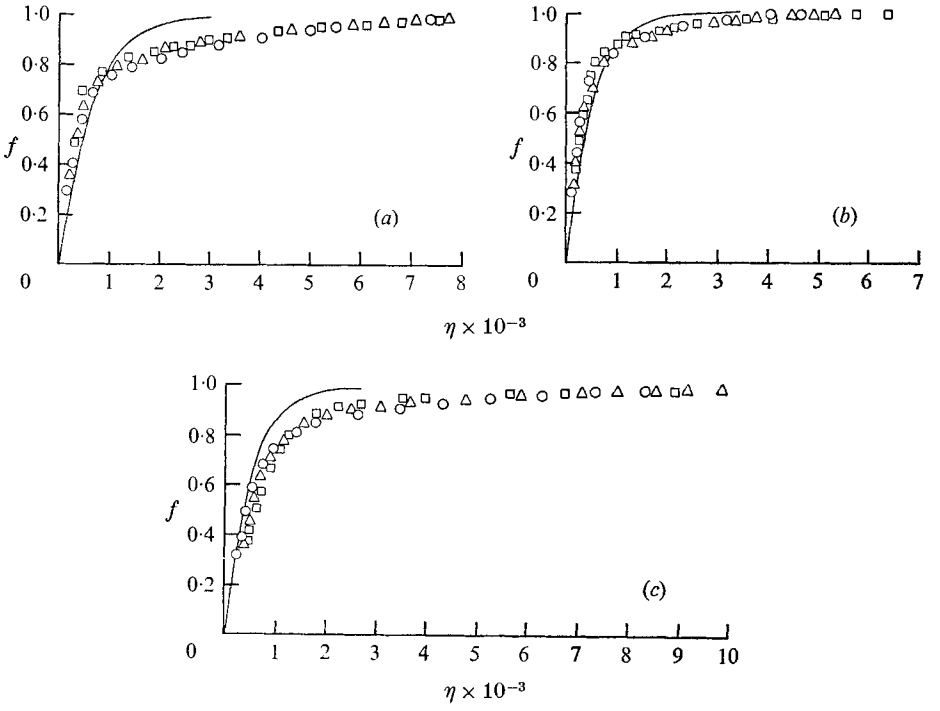

FIGURE 4. Mean velocity profiles in the constant-K acceleration. (*a*) $K = 1{\cdot}5 \times 10^{-6}$. Distance from convergent-channel entrance: ○, 8 in.; △, 16 in.; □, 24 in. ——, laminar solution. (*b*) $K = 2{\cdot}5 \times 10^{-6}$. Distance from convergent-channel entrance: ○, 12 in.; △, 20 in.; □, 28 in. ——, laminar solution. (*c*) $K = 3{\cdot}0 \times 10^{-6}$. Other notation as in (*b*).

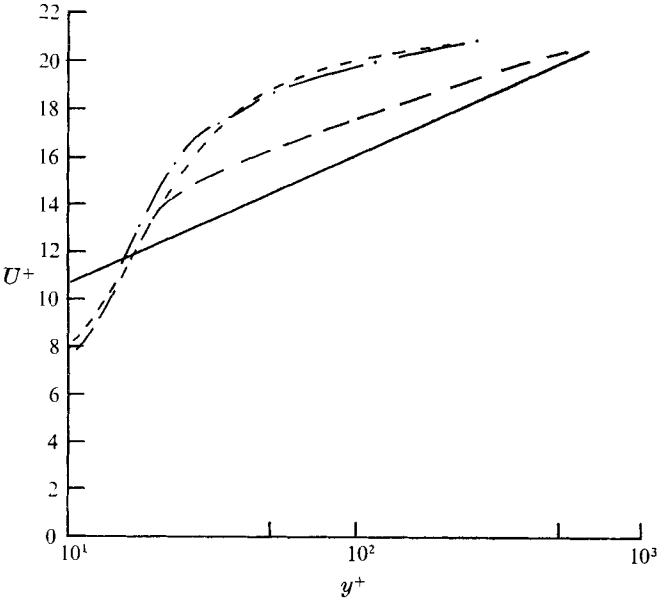

FIGURE 5. Mean velocity profiles in wall co-ordinates. — —, $K = 1{\cdot}5 \times 10^{-6}$; —·—, $K = 2{\cdot}5 \times 10^{-6}$; – – – –, $K = 3{\cdot}0 \times 10^{-6}$; ——, $U^+ = 2{\cdot}44 \ln y^+ + 5{\cdot}0$.

shape from channel entrance to exit. These changes are of course to be expected since the asymptotic structure of the boundary layers will differ from that found at the start of the acceleration.

For $K = 1{\cdot}5 \times 10^{-6}$ and $K = 2{\cdot}5 \times 10^{-6}$ the velocity profiles at different stations show good similarity for f less than about 0·5, i.e. in the vicinity of the wall. The main changes in profile shape occur in the region $0{\cdot}75 < f < 0{\cdot}9$, where a slight filling out of the profile takes place through the acceleration. The velocity profiles corresponding to $K = 3{\cdot}0 \times 10^{-6}$ show somewhat different behaviour in that changes also take place in the vicinity of the wall for $\eta < 10^3$; the velocity profiles appear to become less steep through the acceleration.

In figure 5 mean velocity profiles are plotted on semi-logarithmic axes in U^+, y^+ co-ordinates. Values of C_f obtained from Stanton-tube measurements are used in the normalization. For each value of K a typical mean velocity profile, measured near the end of the acceleration, is plotted. Also shown is the velocity given by Coles's (1962) version of the semi-logarithmic law of the wall. Evidently the velocity profiles lie above the semi-logarithmic wall law by an amount which increases progressively as K is increased. Moreover, it is difficult to draw any clear distinction between the viscous sublayer and the fully turbulent regions of the velocity profiles.

4. Fluctuating quantities

Longitudinal turbulence intensities $(\overline{u^2})^{\frac{1}{2}}/U$ are shown in figure 6 with the similarity variable η as the abscissa variable. Turbulence intensity profiles for each value of the acceleration parameter K are shown at various stations in the constant-K region of the acceleration. For $K = 1{\cdot}5 \times 10^{-6}$, the intensity of about 0·11 occurs near the wall at η equal to approximately 3×10^2 and from this value the intensity falls off rapidly with increasing η in a smooth concave fashion. A small decay in turbulence intensity with distance may be observed in the inner half of the boundary layer, and in the initial part of the acceleration some slight growth (in η co-ordinates) in the thickness of the layer is evident. The profiles do, however, exhibit a fair degree of similarity from station to station throughout the acceleration. A very similar behaviour is displayed by the data obtained at $K = 2{\cdot}5 \times 10^6$ except that here the intensity level diminishes more rapidly with distance from the wall.

For the steepest acceleration, the peak turbulence intensity again occurs for $\eta = 3 \times 10^2$. However, the measurements show a more substantial decay in turbulence intensity through the acceleration than that occurring for the other values of K. This decay is most pronounced in the maximum intensity, in which a decrease of about 25–30 % occurs between the beginning and end of the acceleration. It thus seems likely that the turbulence intensity $\overline{u^2}/U$ profile has not reached its self-preserving form by the end of the acceleration.

For the lowest value of K measurements of Reynolds normal and (non-zero) shear stresses were made at 12 in. from the convergent channel entrance†. The

† The boundary layers for $K = 2{\cdot}5 \times 10^{-6}$ and $3{\cdot}0 \times 10^{-6}$ were considered to be too thin for measurements with an X-wire to yield meaningful results.

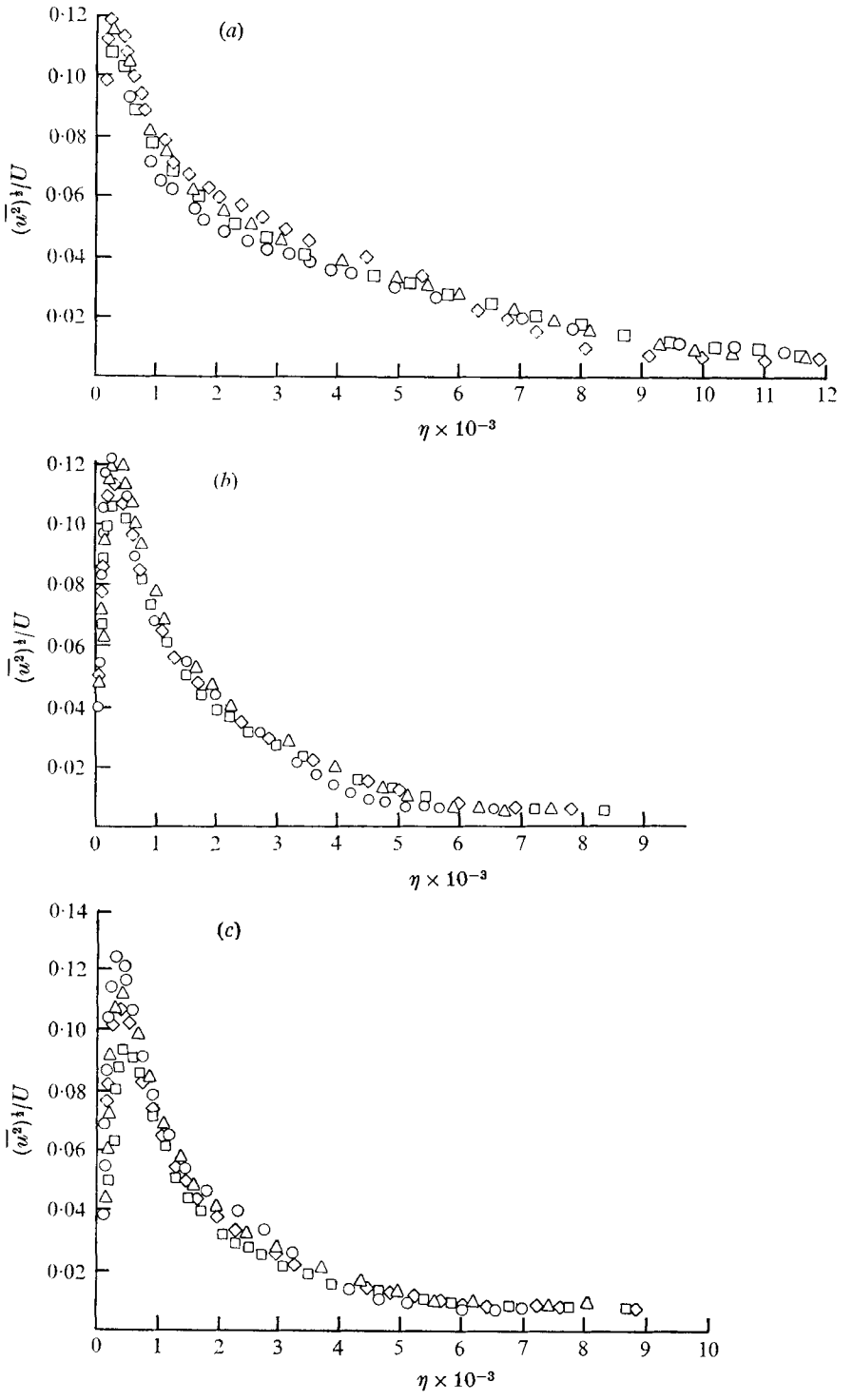

FIGURE 6. Longitudinal turbulence intensity profiles. (*a*) $K = 1{\cdot}5 \times 10^{-6}$. Distance from convergent-channel inlet: ◇, 8 in.; △, 16 in.; □, 20 in.; ○, 24 in. (*b*) $K = 2{\cdot}5 \times 10^{-6}$. Distance from convergent-channel inlet: ○, 12 in.; △, 20 in.; ◇, 24 in.; □, 28 in. (*c*) $K = 3{\cdot}0 \times 10^{-6}$. Other notation as in (*b*).

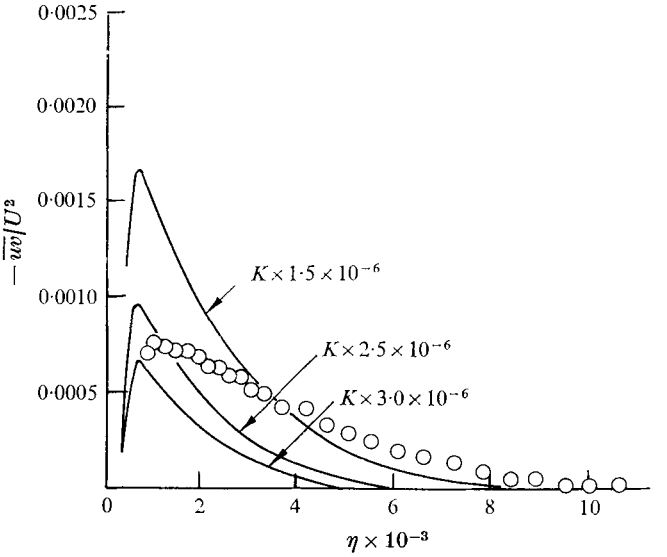

FIGURE 7. Reynolds shear stress profiles for sink-flow boundary layers. ○, X-wire measurements, $K = 1{\cdot}5 \times 10^{-6}$; ——, calculated from (1).

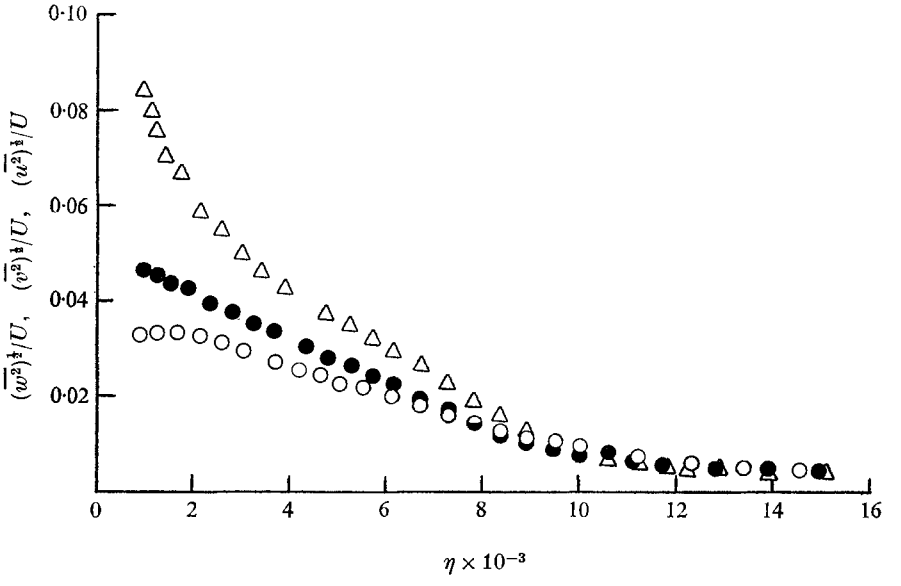

FIGURE 8. Longitudinal, normal and transverse intensity profiles; $K = 1{\cdot}5 \times 10^{-6}$. △, $(\overline{u^2})^{\frac{1}{2}}/U$; ●, $(\overline{v^2})^{\frac{1}{2}}/U$; ○, $(\overline{w^2})^{\frac{1}{2}}/U$.

results of these measurements, which were obtained by traversing an X-wire in the x, z and x, y planes, are shown in figures 7 to 9.

The Reynolds shear stress ($-\overline{uv}$) distribution through the boundary layer is shown in figure 7 with abscissa variable η. The shear stress falls off smoothly with increasing distance from the wall and has its greatest value at the measuring station nearest the wall, where $-\overline{uv}/U^2$ is about 0·0008, a value which is only

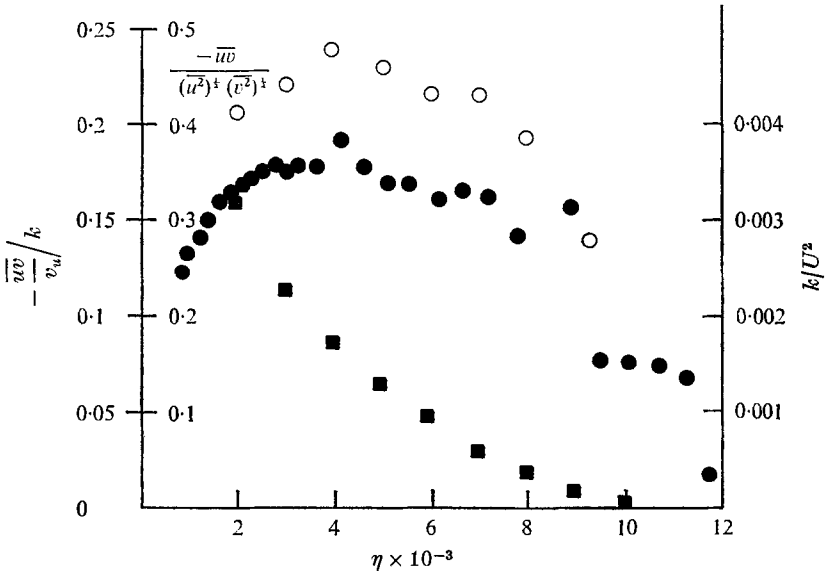

FIGURE 9. Variation of turbulence energy, structure parameter $-\overline{uv}/k$ and coefficient of correlation through the boundary layer; $K = 1{\cdot}5 \times 10^{-6}$. ■, k/U^2; ○, $-\overline{uv}/k$; ●, $-\overline{uv}/(\overline{u^2})^{\frac{1}{2}}(\overline{v^2})^{\frac{1}{2}}$.

about 30 % of the measured wall shear stress. The result is not unexpected, however, since the shear stress will decrease rapidly with increasing distance from the wall in a strongly accelerated flow. Also shown in figure 7 are the Reynolds stress distributions obtained for all three values of K from the measured mean velocity profiles with the aid of the integrated similarity equation (1). For $K = 1{\cdot}5 \times 10^{-6}$ the agreement between the distributions of $\overline{uv}$ obtained by the X-wire and from the mean velocity profile is not particularly good: although both profiles have maximum values considerably less than the wall shear stress there is considerable discrepancy in the detailed profile shapes. Some of this discrepancy is probably due to the shear stress profile not reaching its asymptotic similar form at $x = 12{\cdot}0$ in.; consequently comparison with (1) is not really appropriate.

It emerges from the calculated stress profiles that, as K is increased, the peak turbulent stress becomes a progressively smaller fraction of the wall value: at $K = 1{\cdot}5 \times 10^{-6}$, the maximum value of $-\overline{uv}$ is 70 % of the wall value but only 30 % for the largest value of K.

In figure 8 the r.m.s. values of the Reynolds normal stresses $(\overline{u^2})^{\frac{1}{2}}/U$, $(\overline{v^2})^{\frac{1}{2}}/U$ and $(\overline{w^2})^{\frac{1}{2}}/U$ (w denoting transverse velocity fluctuations) for $K = 1{\cdot}5 \times 10^{-6}$ are shown. Whilst, as noted above, the peak value of $(\overline{u^2})^{\frac{1}{2}}$ is located at $\eta \approx 3 \times 10^2$, the maximum value of $(\overline{v^2})^{\frac{1}{2}}$ appears to occur for $\eta \approx 1{\cdot}5 \times 10^3$. (The peak in $(\overline{w^2})^{\frac{1}{2}}$ was not accessible to our instrumentation.) Near the wall the longitudinal turbulence intensity $(\overline{u^2})^{\frac{1}{2}}/U$ is by far the largest, being about 1·5 times the magnitude of the transverse intensity, which is in turn about 30 % larger than the normal component $(\overline{v^2})^{\frac{1}{2}}/U$. At the outer edge of the boundary layer the three intensities become equal. The intensity measurements shown in figure 8 are in roughly the same proportion to each other as those found in a constant-pressure,

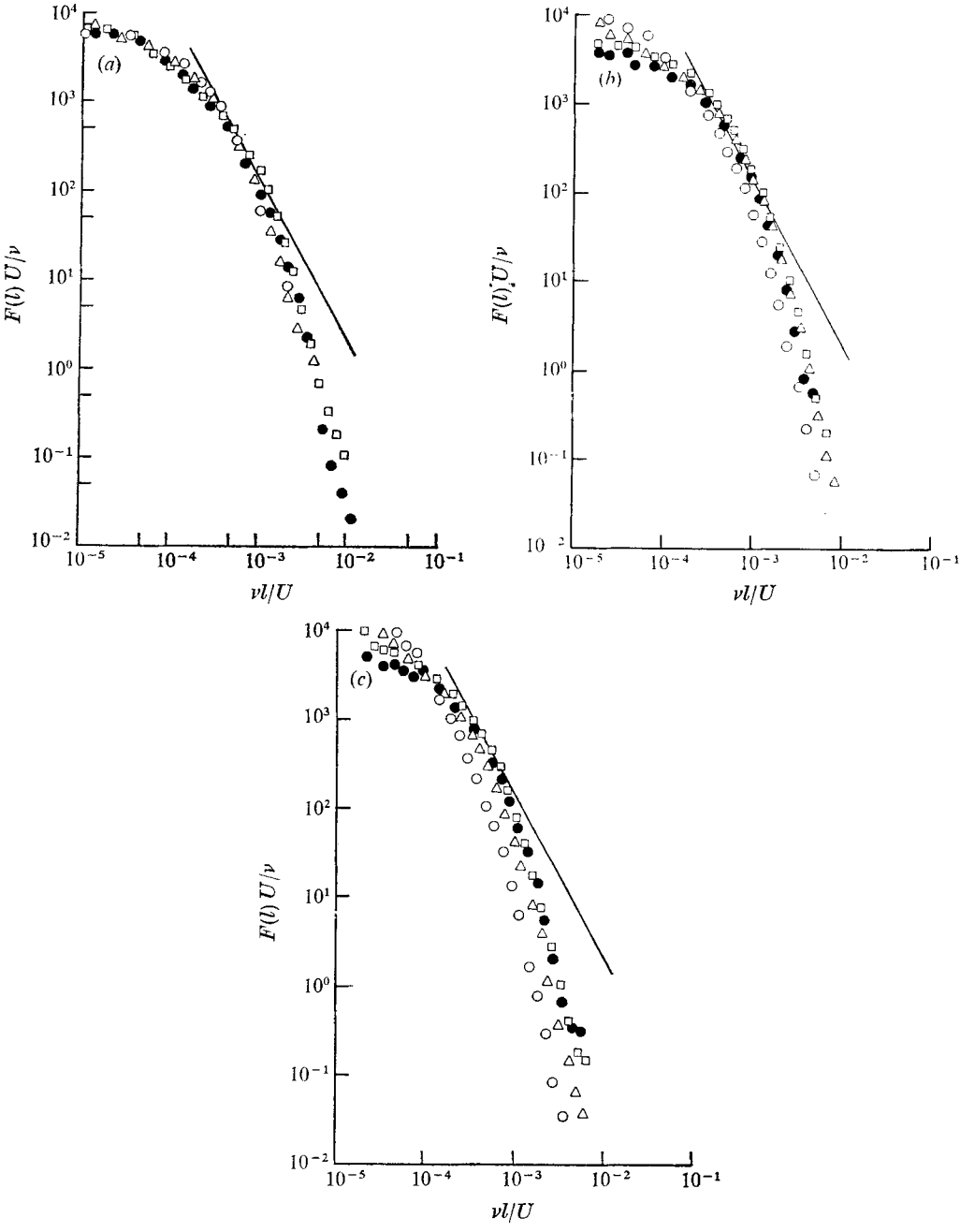

FIGURE 10. Spectra of longitudinal turbulence intensity. ——, $-\frac{5}{3}$ law. (*a*) $K = 1{\cdot}5 \times 10^{-6}$, $x = 20$ in. (*b*) $K = 2{\cdot}5 \times 10^{-6}$, $x = 24$ in. (*c*) $K = 3{\cdot}0 \times 10^{-6}$, $x = 24$ in. Position in layer (η) as follows.

	●	□	△	○
(*a*)	$1{\cdot}0 \times 10^{3}$	$2{\cdot}9 \times 10^{3}$	$5{\cdot}9 \times 10^{3}$	$8{\cdot}8 \times 10^{3}$
(*b*)	$4{\cdot}8 \times 10^{3}$	$3{\cdot}2 \times 10^{3}$	$1{\cdot}6 \times 10^{3}$	$5{\cdot}4 \times 10^{3}$
(*c*)	$4{\cdot}0 \times 10^{3}$	$2{\cdot}8 \times 10^{3}$	$1{\cdot}4 \times 10^{3}$	$4{\cdot}7 \times 10^{3}$

high Reynolds number, turbulent boundary layer, e.g. Klebanoff (1954). However, the intensities of figure 8 fall off more rapidly than in the constant-pressure case. This difference is mainly attributable to the relative difference in the shear stress distribution in constant-pressure and strongly accelerated flows.

By way of illustration, profiles of the turbulence kinetic energy k/U^2, the correlation coefficient $-\overline{uv}/(\overline{u^2})^{\frac{1}{2}}(\overline{v^2})^{\frac{1}{2}}$ and the structure parameter $-\overline{uv}/k$ are plotted with abscissa variable η in figure 9. The turbulence kinetic energy profile follows the expected form, decreasing smoothly with increasing distance from the wall. The structure parameter $-\overline{uv}/k$ and correlation coefficient are both approximately constant over about 75 % of the boundary layer. However, their magnitudes are some 25 % less than the values commonly found in high Reynolds number boundary layers.

At each level of acceleration, spectra of $\overline{u^2}$ were measured at several positions in the boundary layer and at several stations. The data at the positions furthest downstream are representative of those at other positions and only these have been included in figure 10; more extensive comparisons are provided by Jones (1971). The spectra, which are normalized by the mean-flow velocity and length scales, U and ν/U, cover positions in the range $0{\cdot}1 < y/\delta < 1{\cdot}0$, δ denoting the boundary-layer thickness.

For all values of K, the spectra at different positions in the boundary layer have essentially the same shape, indicating a rather uniform structure across the boundary layer. In none of the spectra is there a region displaying a $-\frac{5}{3}$ decay law; in view of the low Reynolds numbers of these flows, however, the result is expected. For K equal to $1{\cdot}5 \times 10^{-6}$, the spectra are, to all intents, quite independent of position, a result which suggests that the length scales of turbulent motion are sensibly constant across the flow. The same is true for the outer three spectra in the boundary layers with the steeper accelerations. However, the near-wall spectra indicate a substantial increase in the longitudinal length scales of the turbulence near the wall. In view of this unexpected result it is pertinent to add that the same behaviour was also displayed, for both values of K, for stations farther upstream (Jones 1971). Because spectra data of the kind presented above provide such an incomplete representation of the flow structure we shall not attempt here an explanation of the result.

Lastly, and perhaps most interestingly, the changes which occur in the spectra shape as K is progressively increased are remarkably like those measured in the viscous-dependent region of say a high Reynolds number channel flow as one moves progressively closer to the wall (e.g. Comte-Bellot 1965).

5. Concluding remarks

The data presented above should provide a fairly searching test of any transport hypothesis that may be developed for low Reynolds number turbulence. Qualitatively they exhibit the same trends as do those of earlier investigations; in detail, however, there are a number of differences. The asymptotic Reynolds numbers and shape factors are somewhat at variance with the data of Julien *et al.* and Loyd *et al.*, and our data suggest unequivocally that a turbulent

sink-flow boundary layer may be set up for values of K as high as $2{\cdot}5 \times 10^6$. On one matter there is general concurrence, however, and that is the level of the skin-friction coefficient. All the credible data suggest that C_f is sensibly constant, with a value of about 0·0050, for values of K above 10^{-6}. This value it will be noted is practically the same as that suggested by Coles (1962) as the maximum attainable in a boundary layer in a zero pressure gradient.

Just what the maximum level of acceleration is in which a turbulent flow may be sustained has not been resolved by the present work. Perhaps the best that can be said is that the critical value is at least $2{\cdot}5 \times 10^{-6}$ and probably below $3{\cdot}5 \times 10^{-6}$ (above which value Schraub & Kline (1965) observed that streak formations in the sublayer were completely suppressed). Future experimenters should certainly succeed in narrowing this band of uncertainty but to avoid the kinds of doubt which attach, for example, to our own data for $K = 3 \times 10^{-6}$ their apparatus will need to be of a quite different scale from those hitherto employed. What is needed is a velocity ratio between exit and inlet of 10:1 and an asymptotic boundary layer at least one inch in thickness. These criteria in turn suggest a low inlet velocity, a small convergence angle (and hence a very long test section) and, perhaps, a working fluid other than air.

We acknowledge the support by the Science Research Council (contract B/SR/5049), of this research. Mr P. Bradshaw loaned us several instruments and Dr F. J. Durst provided helpful advice on signal processing; to them we offer our sincere thanks.

REFERENCES

Badri Narayanan, M. A. & Ramjee, V. 1968 On the criteria for reverse transition in a two-dimensional boundary-layer flow. *India Inst. Sci. Rep.* AE 68 FM 1.

Bradshaw, P. 1965 A compact null-reading, tilting U-tube micromanometer with a rigid liquid container. *J. Sci. Instrum.* **42**, 677.

Champagne, F. H., Sleicher, C. A. & Wehrmann, O. H. 1967 Turbulence measurements with inclined hot wires. *J. Fluid Mech.* **28**, 153.

Coles, D. E. 1956 The law of the wake in a turbulent boundary layer. *J. Fluid Mech.* **1**, 191.

Coles, D. E. 1957 Remarks on the equilibrium turbulent boundary layer. *J. Aero. Sci.* **24**, 495.

Coles, D. E. 1962 The turbulent boundary layer in a compressible fluid. *Rand Rep.* 403-PR.

Comte-Bellot, G. 1965 Ecoulement turbulent entre deux parois parallèles. *Publ. Sci. Tech. Minst. de l'Air.*

Herring, H. J. & Norbury, J. F. 1967 Experiments on equilibrium turbulent boundary layers in favourable pressure gradients. *J. Fluid Mech.* **27**, 541.

Jones, W. P. 1967 Strongly accelerated turbulent boundary layers. M.Sc. thesis, University of London.

Jones, W. P. 1971 Laminarization in strongly accelerated boundary layers. Ph.D. thesis, University of London.

Julien, H. L., Kays, W. M. & Moffat, R. J. 1969 The turbulent boundary layer on a porous plate: experiment study of the effects of a favourable pressure gradient. *Stanford University, Thermo. Sci. Div. Rep.* HMT-4.

Klebanoff, P. S. 1954 *N.A.C.A. Tech. Note*, no. 3178.

LAUNDER, B. E. & JONES, W. P 1969 Sink-flow turbulent boundary layers. *J. Fluid Mech.* **38**, 817.

LAUNDER, B. E. & STINCHCOMBE, H. S. 1967 Non-normal similar boundary layers. *Imperial College, Mech. Engng Dept. Rep.* TWF/TN/21.

LOYD, R. J., MOFFAT, R. J. & KAYS, W. M. 1970 The turbulent boundary layer on a porous plate: an experimental study of the fluid dynamics with strong favourable pressure gradients and blowing. *Stanford University, Thermo. Sci. Div. Rep.* HMT-13.

MCMILLAN, F. A. 1956 Experiments on pitot tubes in shear flow. *Aero. Res. Counc. Rep.* no. 3028.

PATEL, V. C. 1965 Calibration of Preston tube and limitations of its use in pressure gradients. *J. Fluid Mech.* **23**, 185.

SCHRAUB, F. A. & KLINE, S. J. 1965 *Stanford University, Mech. Engng Dept. Rep.* MD-12.